Isotope Effects in Electron Transfer across the Electrode−Electrolyte Interface: A Measure of Solvent Mode Quantization

August Calhoun and Gregory A. Voth*

Department of Chemistry and Henry Eyring Center for Theoretical Chemistry, University of Utah, Salt Lake City, Utah 84112

Received: June 15, 1998; In Final Form: August 14, 1998

The free energy of electron transfer (ET) is computed for the electrochemical Fe^{2+}/Fe^{3+} reaction with a Pt electrode. The quantum mechanical effects of the solvent nuclei are included via the method of path integral quantum transition state theory (PI-QTST). The effect of isotopic substitution (deuterium for hydrogen) on the ET rate constant at zero overpotential is investigated by analyzing the change in the quantum free energy barrier for ET. The results exhibit an inverse isotope effect, and interestingly, the isotope effect is primarily due to changes in the second and third water solvation shells around the iron ion.

1. Introduction

Electron transfer (ET) across the electrode/electrolyte interface is the central kinetic step in electrochemistry. Experimental characterization of the microscopic events involved in the electron-transfer process is complicated by the dielectric interface, which can interfere with kinetic and spectroscopic measurements. A growing body of theoretical and simulation work has been devoted to exploring electrochemical ET (see, for example, refs 1−12); however, the phenomenon is far from completely understood. Such studies have nevertheless resulted in a clearer picture of the microscopic events that affect ET. For example, simulations from this group[3] have shown a good agreement with experiment[13] for the free energy barrier to electron transfer in a dilute ferrous−ferric solution at a platinum electrode. In addition, insight has been gained into counterion effects that may influence experimental measurements of the rate of ET.[3,13] Other simulations have illustrated the importance of properly accounting for the quantum nature of water within ET simulations.[2]

In the present work, we build upon this body of work by directly addressing manifestations of the quantum mechanical nature of the solvent. This is accomplished by computing the isotope effect on the free energy barrier for ET. Classically, there is only a small isotope effect on the free energy barrier when D_2O is substituted for H_2O because the solvent free energy barrier does not depend on the mass. Quantum mechanically, however, the particle mass does directly enter into the calculation because of the noncommutation of the position and momentum operators. The resulting isotope effect should be experimentally observable by conducting experiments to measure the ET rate for both water and heavy water at zero overpotential. To our best knowledge, this effect has not been measured to date, in part because of the difficulties associated with counterion absorption to the electrode surface.

The present paper is organized as follows. In section 2 the microscopic model that underlies the calculation is presented. Then in section 3 the simulation results are given. Concluding remarks appear in section 4.

2. Model

The molecular dynamics (MD) model in the present investigation is in many ways similar to that in to our earlier work[2] but with significant improvements in the treatment of the electrostatic boundary conditions. A ferric ion, solvated by an explicit water model, is fixed above a metal electrode surface. An electron is effectively shared between the ion and the electrode surface via the Anderson−Newns Hamiltonian.[8,14−16] This formalism describes a single electronic state on the ferric ion coupled to the metal electrode states, and it can be readily incorporated into MD or path integral molecular dynamics (PIMD) simulations. From these simulations,[2] one may compute the adiabatic free energy of ET for the reaction $Fe^{3+} + e^- \rightarrow Fe^{2+}$. The following subsections shall summarize the Anderson−Newns Hamiltonian approach, outline our PIMD methodology, and describe the simulation model in detail.

Anderson−Newns Approach. The Anderson−Newns Hamiltonian is solved within the Born−Oppenheimer approximation to give[2−4]

$$H = H_{\text{solvent}} + E_0(\Delta E) \tag{1}$$

where H_{solvent} is the solvent−solvent and solvent−electrode part of the Hamiltonian, and $E_0(\Delta E)$ is the ground-state solution of the electronic Hamiltonian given by

$$E_0(\Delta E) = Z\Delta E - \frac{\Delta E}{2} + \frac{1}{\pi}(\epsilon_a - \Delta E - \epsilon_F)\tan^{-1}\left(\frac{\epsilon_F - \epsilon_a + \Delta E}{\Delta}\right) + \frac{\Delta}{2\pi}\ln[(\epsilon_a - \Delta E - \epsilon_F)^2 + \Delta^2] \tag{2}$$

The parameter Δ in this equation is the coupling between the redox ion electronic level and the electrode, and ΔE is a collective solvation variable explicitly described below. The above expression can be readily incorporated into MD or PIMD simulations because it is a function of the nuclear positions of the system only.[2−4] The experimental value of the ion orbital

10.1021/jp982633u CCC: $15.00
Published on Web 10/02/1998

energy level, ϵ_a, can be used, and Δ can be computed from ab initio methods[17,18] or estimated. The Fermi level, ϵ_F, is an adjustable parameter, and it can be related to the electrode overpotential. The electronic energy and average population are thus a unique function of the collective solvent reaction coordinate,[2]

$$\Delta E = -(V_{\text{solvent-ion}} - V_{\text{solvent-ion image}}) \tag{3}$$

which is defined in the traditional Marcus picture as[3]

$$\Delta E = -\left(\sum_i^N \frac{q_i e}{r_{i,\text{ion}}} - \sum_j^N \frac{q_j e}{r_{j,\text{image}}}\right) \tag{4}$$

This function is the sum of all of the solvent charge (q_i) interactions with a unit electronic charge at the redox ion site (e) and the redox image [reflected through the metal surface in the perfect conductor approximation for the metal ($-e$)].[3] It can also be thought of as a difference potential, where the only change between the two electronic states is the ionic charge. Molecular dynamics simulations can then be performed with the Hamiltonian in eq 2.

An important quantity in the present work is the electrode overpotential, η, which is equal to the thermodynamic driving force for the ET reaction ΔG. The experimental conditions for measuring the rate of ET often correspond to zero electrode overpotential, and therefore, the present work will compute the free energy barriers for such conditions. It has been shown that for a linearly responding solvent the overpotential is given by[8]

$$\eta = \epsilon_a - \epsilon_F + \Delta e_{\text{min}} - \lambda \tag{5}$$

where Δe_{min} minimum of the right-hand well of the free energy curve (ferric state), and λ is the reorganization free energy. This is a useful approximation for the present simulations in order to estimate the Fermi level that will give solvent-free energy curves with zero overpotential.

B. Quantum Water. The quantization of the model for water was carried out by the method of imaginary time Feynman path integrals. This is a convenient and often used tool for calculating equilibrium quantum mechanical properties of finite temperature systems (see, for example, ref 19). The formulation of the problem via a Feynman path integral method scales much more favorably with the number of degrees of freedom than a formulation based upon the Schrödinger equation. This makes the method particularly useful for condensed matter systems.

The present simulations were carried out using the "primitive" discretization[19] and path integral molecular dynamics (PIMD) for the quasiparticle configurational sampling. The path integral solvent could thus be employed in a transparent manner within the MD model. There are a number of simulation studies that have used path integral water models to calculate various properties for aqueous systems. These studies have utilized both flexible and rigid water models, and the original papers include a far more detailed discussion of the implementation than is presented here.[2,20-26]

C. Simulation Model. The water model used in the present simulation is a derivative of the simple point charge (SPC) model for water (SPC is a rigid model).[27] A flexible version of SPC with a harmonic intramolecular potential for the oxygen−hydrogen and the hydrogen−hydrogen distances is known as SPC/F.[28] The SPC/F model has been reparametrized such that the Fourier transform of the quantum velocity autocorrelation function gives a much better approximation to the experimental infrared spectrum of water, so the dielectric constant is in better agreement with experiment. This quantum model for water is called SPC/F_2.[20] In this work we employ the SPC/F_2 model for water because it was specifically parametrized for use in quantum path integral simulations.

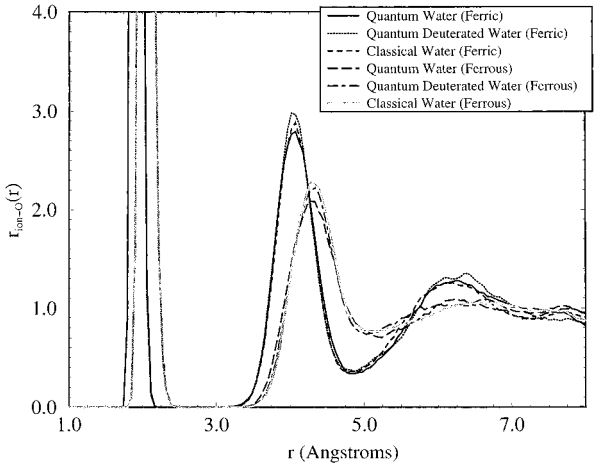

Figure 1. Ion−oxygen radial distribution function in bulk classical and quantum water. The oxygen distribution is shifted toward the ion, but the area under the first peak, which is proportional to the number of water molecules in the first solvation shell, remains the same. This is a characteristic of an outer-sphere ET reaction.

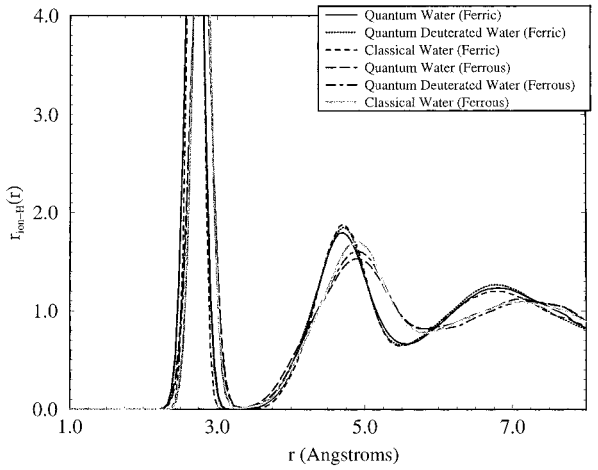

Figure 2. Ion−hydrogen radial distribution function in bulk classical and quantum water.

The ferric ion was fixed 5.5 Å above a corrugated Pt(111) surface[29-31] because this was found to be the equilibrium height of the ion above the metal surface. The water−ion interaction was the same as in previous studies,[2,3,32-34] and the water−ion pair distribution functions are shown in Figures 1 and 2. Note that the first peak is shifted toward the ion for the ferric (+3) ion, but the area under the first peak, which is proportional to the number of waters in the first solvation shell, is the same. This is a characteristic of an outer-sphere ET reaction.[35] The vacuum energy of the ferric ion orbital, ϵ_a, was chosen to be the experimental value of 30.561 eV, and the value of Δ was estimated to be 0.0355 eV.[3,17,18] A total of 320 SPC/F_2 water molecules were included in the molecular dynamics cell, which had dimensions of 24.93 Å × 19.16 Å × 42.33 Å (*xyz*). The MD cell is shown in the schematic diagram in Figure 3. The water molecules were restricted to be in the top half of the molecular dynamics cell by the metal surface, and the image of the ion core and of the electronic population on the redox ion was reflected through the metal surface in the perfect

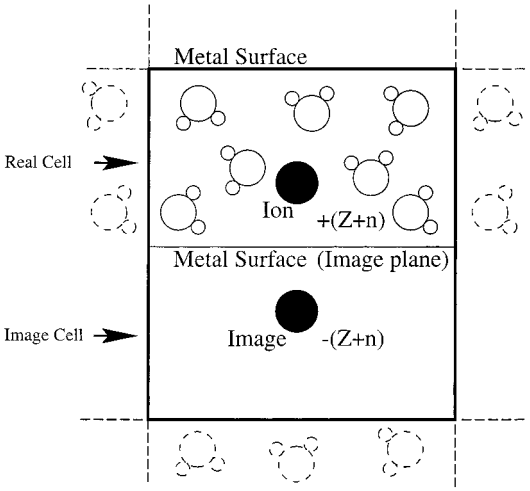

Figure 3. Schematic of the cell utilized in the MD simulations. The image of the redox ion is reflected through the image plane (the metal surface). Images of the water molecules are not explicitly included, since they are accounted for in a static way by the Pt−water potential. The entire supercell (comprised of the real cell plus the image cell) is replicated in three dimensions via the Ewald summation. The charge on the ion at any given time is $Z + \langle n \rangle$, where Z is the core charge on the ion and $\langle n \rangle$ is the population on the orbital on the ion. This instantaneous value determines the magnitude of the image charge.

conductor approximation for the electrode.[4] The charge on the ion at any given instant is $Z + \langle n \rangle$, where Z is the core charge of the ion (+3 in this case), and $\langle n \rangle$ is the instantaneous electronic charge of the redox ion orbital. This instantaneous total charge on the ion determines the magnitude of the image charge as well, which is equal and opposite the ion's charge. The solvent, therefore, interacts with the ion and the ion image, both of which have a variable charge. The images of the water molecules were not included in the present model because this effect is accounted for in a static way by the water−metal interaction.[30,31] The entire molecular dynamics cell was replicated in three dimensions via the Ewald summation method, which, including the ion image, results in a charge neutral cell.[36] Periodic boundary conditions were used, and the z dimension of the box size was adjusted to yield the bulk density of water in the center. The x and y dimensions were chosen to be commensurate with an integer number of Pt(111) unit cells.[2,29−31] The equations of motion were integrated with a force split multiple time step algorithm based on the velocity Verlet method,[37−39] and a Nose−Hoover chain of length 2 was attached to each quasiparticle for temperature control and ergodic sampling.[40,41] A small time step of $^1/_8$ fs was used to integrate the PIMD harmonic spring and water intramolecular motions, and a large time step of 1 fs was used to integrate the equations of motion for the intermolecular motions. The fictitious mass of the hydrogen quasiparticles was chosen to be 500 electron mass units.

The number of path discretizations for the quantum simulations, P, was chosen based on a Monte Carlo path integral simulation of a water dimer held together by a harmonic potential.[2,20] The internal potential energy as a function of P was computed because this quantity was the most sensitive with respect to convergence of P. The values employed in the present simulations are $P = 25$ for quantum water and $P = 14$ for quantum deuterated water.[2,20]

3. Results: Free Energy Curves and the Isotope Effect

The free energy of ET was computed from the system described above with classical, quantum, and quantum deuterated water. The free energy can be written as a configurational average[2−4]

$$F(\Delta e) = -k_B T \ln[\int d\mathbf{q}\, \delta[\Delta e - \Delta E(\mathbf{q})]\, e^{-\beta H(\mathbf{q})}] \quad (6)$$

where Δe is a particular value of the collective reaction coordinate and $\mathbf{q}$ is a multidimensional vector of all the system coordinates. Umbrella sampling was utilized to sample the free energy curve. A harmonic umbrella potential of the form

$$V_{\text{umbrella}}(\Delta e) = \frac{k}{2}(\Delta e - \Delta e_0)^2 \quad (7)$$

was used to sample "windows" of the free energy along the collective solvent reaction coordinate.[42] The umbrella potential was then rigorously removed from the simulation data, and the pieces of the free energy curve matched. A least-squares fit to the simulation data was employed which takes a weighted average over the statistics from each separate simulation into account when matching the free energy windows.[43,44]

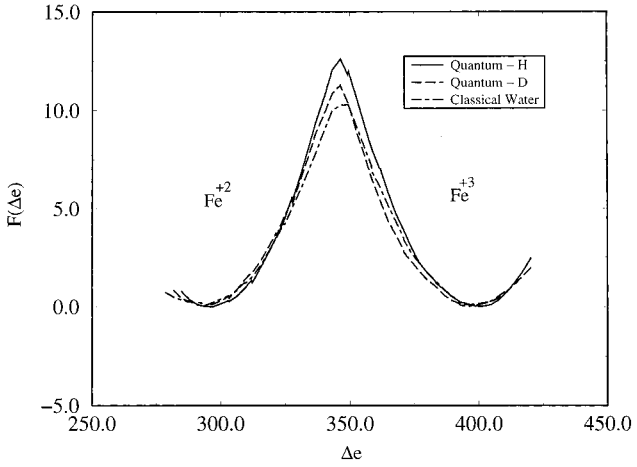

Figure 4. Adiabatic free energy curves for quantum water, D_2O, and classical water.

A total of 14 free energy windows were used to construct each free energy curve in Figure 4. First, the classical free energy curve was computed because it was computationally the least demanding. Each free energy window was equilibrated for 20 ps, and free energy data were then collected for 20 ps. Several curves were constructed, and the Fermi level parameter in the Anderson−Newns Hamiltonian was adjusted based on the basis of for each curve such that the subsequent one was closer to zero overpotential. The resulting (approximately symmetric) free energy barrier can then be properly compared to experimental results. This required five iterations of the process of computing the free energy curve and then adjusting the Fermi level for the classical water. The quantum water simulations could be initiated with a better initial guess for the Fermi level because the appropriate value for the classical water case was known. Thus, the quantum H and D curves only had to be recomputed once to achieve approximately zero overpotential. The results are shown in Figure 4.

The quantum free energy windows for the H and D simulations were each equilibrated for 10 ps and averaged for 10 ps. The quantum simulations were started from the classical configurations with a random quasiparticle distribution centered about the classical particle position. The width of the distribution was chosen to be equal to half of the quantum thermal wavelength of the H or D computed in the free particle approximation. The statistical errors in the free energy curves

TABLE 1: Parameters for the Harmonic Fits to the Right-Hand Wells of the Adiabatic Free Energy Curves[a]

solvent	reorganization free energy λ (kcal/mol)	minimum Δe_{min} (kcal/mol)	overpotential, η (kcal/mol)	Fermi level, ϵ_F (kcal/mol)
quantum H	59.0	401.3	0.05	360.5
quantum D	58.5	400.3	0.03	359.4
classical	57.7	399.2	0.01	358.8

[a] The statistical errors are approximately 0.3 kcal/mol in the reorganization energy and the minimum. The Fermi level used to generate each free energy curve is shown as well.

TABLE 2: Free Energy Barriers for the $Fe^{3+} + e^- \rightarrow Fe^{2+}$ ET Reaction from the Simulation Data

solvent	oxidation barrier (kcal/mol)	reduction barrier (kcal/mol)
quantum H	12.9 ± 0.2	12.6 ± 0.2
quantum D	11.1 ± 0.1	11.1 ± 0.1
classical	10.1 ± 0.1	10.1 ± 0.1

are approximately 0.2 kcal/mol. This was computed from the standard deviation for each point by breaking up the free energy calculation into different averaging intervals. All errors were computed by propagation of errors.

The parameters from the harmonic fits to the right-hand wells of Figure 4 are given in Table 1. These harmonic fits are used within a linear response approximation to eq 1 in which $H_{solvent}$ is approximated as

$$H_{solvent} \approx \frac{(\Delta E - \Delta e_{min})^2}{4\lambda} \tag{8}$$

The final values of the Fermi level used to generate the free energy curves are shown in Table 1 as well. The statistical errors in the harmonic fits, and hence λ and Δe_{min}, of the free energy curves are approximately 0.3 kcal/mol.

The magnitude of the barrier for each curve is given in Table 2. The overpotential is not exactly zero for any of the free energy curves, so the magnitude of this difference is a systematic error in our calculations. From inspection of the free energy barriers, one can see that the effect is an *inverse* isotope effect. That is, the barrier to ET is larger for H_2O than for D_2O. This is not what one would expect from simple quantum mechanical estimates based on nuclear tunneling, which would lower the barrier more for H_2O than for D_2O. This calculated effect is, however, understandable within the present model. The dipole moment of the H_2O is larger than that of D_2O near the ion because hydrogen nuclei have a larger delocalization than deuterium. The SPC/F_2 model for H_2O is, therefore, effectively more polarizable than for D_2O. This effect is enhanced near the ion and is shown by the shift of the minimum of the right-hand free energy well to higher energy for the quantum water as seen in Table 1. In the first solvation shell, the average O−H bond length of the H_2O is 1.16 ± 0.01 Å compared to 1.13 ± 0.01 Å for D_2O, leading to a larger effective dipole in the point charge model. The quantum water can thus solvate the ion better than the quantum deuterated water because of its enhanced effective polarizability and dipole moment. The enhanced polarizability of a quantum model for water has also recently been observed in diffusion Monte Carlo calculations for a water dimer.[45]

Further away from the ion, the effect of the hydrogen and deuterium quantization can also be seen in the ion−oxygen and ion−hydrogen (deuterium) radial distribution functions shown in Figures 1 and 2. A broadening and shift inward of the second peak in the ion−oxygen radial distribution function can be seen for the quantum water versus the D_2O and classical water cases. The second peak of the quantum ion−hydrogen radial distribution function is also broadened and shifted toward the ion relative to the quantum deuterated and classical water. The effect is mostly due to the second and third solvation shells, and this can be more clearly seen in a plot of the ion coordination number (i.e., the integral over the radial distribution function) given by

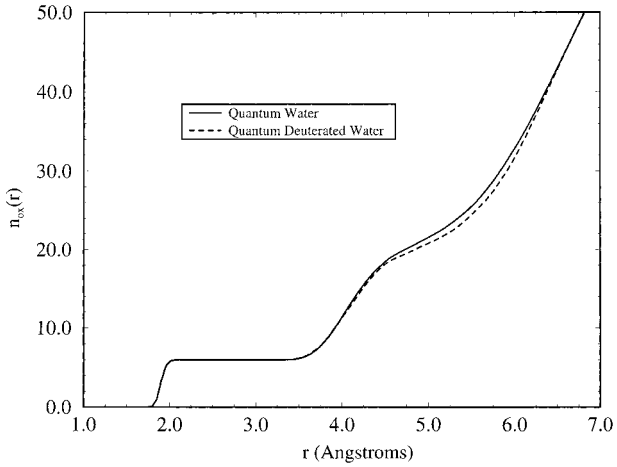

Figure 5. Oxygen coordination number around the ferric ion for quantum water and quantum deuterated water. Note that the differences are in the second and third solvation shells.

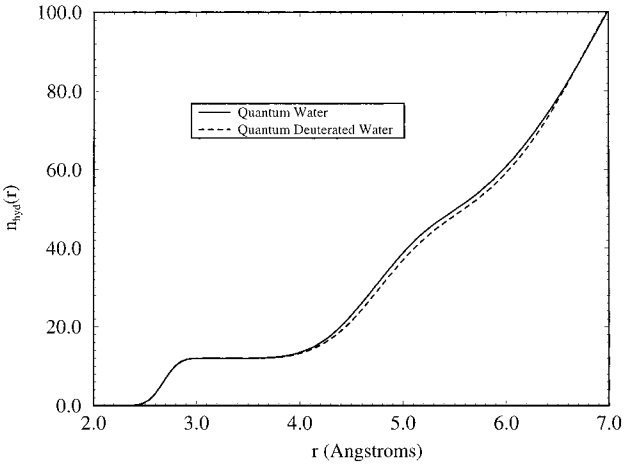

Figure 6. Hydrogen coordination number around the ferric ion for quantum water and quantum deuterated water. Note that the differences are in the second and third solvation shells.

$$n(r') = 4\pi\rho \int_0^{r'} g(r) r^2 \, dr \tag{9}$$

The oxygen and hydrogen coordination numbers are shown as a function of r (the distance from the ferric ion) in Figures 5 and 6 (where ρ is the density of water). Qualitatively, this means that any attempt to treat only part of this system quantum mechanically would require including at least the second and third solvation shells in the quantum mechanical part of the Hamiltonian, not just the first ligand shell.

A direct estimate of the shift of the minimum of the solvent free energy curve due to the quantum effects may be obtained via thermodynamic integration. This technique consists of introducing an auxiliary variable λ, which scales relevant interactions in or out of a Hamiltonian. This constructs an artificial path between two states, thereby allowing the direct

calculation of the free energy difference between those states. In the present application, the differences between the quantum and classical minimum of the free energy curve are directly due to the quantum effects. The action of the imaginary time path integral is given by[2,19]

$$\frac{S}{\beta} = \sum_{i=1}^{P} \left[\frac{mP}{2\beta^2}(x_{i+1} - x_i)^2 + \frac{1}{P}V(x_i) \right] \tag{10}$$

The classical limit is to replace the second term in the brackets by the centroid of the quasiparticles; hence, the classical limit action is[46]

$$\frac{S_{cl}}{\beta} = \sum_{i=1}^{P} \left[\frac{mP}{2\beta^2}(x_{i+1} - x_i)^2 + \frac{1}{P}V(x_0) \right] \tag{11}$$

where x_0 is the centroid, which is defined as

$$x_0 = \frac{1}{P}\sum_{i=1}^{P} x_i \tag{12}$$

An artificial path can therefore be constructed between the quantum and classical limits, and the free energy difference can be computed. The thermodynamic integration parameter λ is utilized to introduce the quantum effects, and the action integral can be written as

$$\frac{S_\lambda}{\beta} = \sum_{i=1}^{P} \left[\frac{mP}{2\beta^2}(x_{i+1} - x_i)^2 + V(x_0) \right] + \lambda\left(\frac{1}{P}\sum_{i=1}^{P} V(x_i) - V(x_0) \right) \tag{13}$$

The free energy difference may be computed by first evaluating

$$\left\langle \frac{\partial H}{\partial \lambda} \right\rangle_\lambda = \left\langle \frac{1}{P}\sum_{i=1}^{P} V(x_i) - V(x_0) \right\rangle_\lambda \tag{14}$$

for various values of λ and evaluating the integral

$$\Delta F = \int_0^1 d\lambda \left\langle \frac{\partial H}{\partial \lambda} \right\rangle_\lambda \tag{15}$$

The free energy difference due to the quantum corrections to the ion−solvent interactions was computed for H_2O and D_2O. Ten values of λ between 0 and 1 were chosen, equilibrated for 10 ps, and data collected for 30 ps. The simulations were conducted while the system was in the ferric state (right well of the free energy curve). The results were found to be $\Delta F_{H_2O} = 1.9$ kcal/mol and $\Delta F_{D_2O} = 0.8$ kcal/mol. The errors were approximately 0.5 kcal/mol for both solvents. This result agrees within the statistical errors with the observed shift of the minimum of the solvent free energy curves from the umbrella sampling calculations, which was 2.1 kcal/mol for H_2O and 1.0 kcal/mol for D_2O (see Table 1). This result confirms our hypothesis that the difference in the free energy barriers is primarily due to the difference in solvation of the iron ion by the quantum H_2O and D_2O solvents.

The larger shift of the minimum of the free energy curve for the quantum water, relative to D_2O, raises the barrier height more for the quantum water than the quantum deuterated water. The quantum water model barrier for oxidation is 12.9 ± 0.5 kcal/mol, which compares very favorably with the experimentally measured barrier of 13.5 ± 0.4 kcal/mol.[13] Unfortunately, the authors are not aware of any experimental studies where direct isotope effects have been measured, or the free energy of ET measured for a D_2O solvent.

The isotope effect on the *rate constants* may be computed by comparing the ratio of the path integral quantum transition-state theory (PI-QTST) estimates of the rate constants for ET in H_2O to that in D_2O, i.e.,

$$\Gamma = \frac{\omega_H e^{-\beta\Delta F^*_H}}{\omega_D e^{-\beta\Delta F^*_D}} = \sqrt{\frac{\mu^{eff}_{D_2O}}{\mu^{eff}_{D_2O}}} \frac{e^{-\beta\Delta F^*_H}}{e^{-\beta\Delta F^*_D}} \tag{16}$$

where ΔF^*_H and ΔF^*_D are the ET free energy barriers in H_2O and D_2O, respectively, and the effective masses, $\mu^{eff}_{D_2O}$ and $\mu^{eff}_{D_2O}$, were computed from the relation

$$\mu_{eff} \approx \frac{k_B T}{\langle \Delta \dot{E}^2 \rangle_{cl}} \tag{17}$$

Here, the average is performed in the classical limit, consistent with PI-QTST, for H_2O and D_2O. The result of the estimate based on eq 17 is $\Gamma = 0.06 \pm 0.01$, which is clearly an inverse effect. The classical isotope effect would be the mass factor in eq 16 only (no difference in the free energy barriers), which is calculated to be 1.21 ± 0.01, i.e., the normal classical isotope effect. Therefore, the quantum isotope effect reduces the rate by a factor of 20 over the classical limit.

It should be noted that the present calculation is fundamentally different from that of Bader et al.,[34] which gave a normal (tunneling) isotope effect for the Fe^{2+}/Fe^{3+} self-exchange reaction in water. Our result is for a *heterogeneous* ET reaction, while the system Bader studied was a symmetric *homogeneous* ET reaction in bulk water. The self-exchange system cannot show the preferential quantum solvation of either ET state as does the heterogeneous ET reaction because of the broken symmetry of the latter. Another important difference is their choice of a rigid SPC water model, which does not allow the intramolecular degrees of freedom to relax in the presence of the ion as does the present flexible water model.

4. Concluding Remarks

In this paper, the isotope effect on the rate of electron transfer between a ferric ion and a Pt electrode was estimated via path integral molecular dynamics and PI-QTST. The ratio of the probability to be at the top of the free energy barrier was used to quantify the isotope effect. The free energy curves for quantum water and for D_2O were constructed via umbrella sampling. The results exhibit a pronounced inverse isotope effect, which is due to the better solvation of the ion by the quantum water rather than by D_2O. The free energy barrier computed from the simulation of quantum water is in good agreement with the experimental value; however, the experimental isotope effect in the heterogeneous ferrous−ferric reaction is not yet known. It is noteworthy that the isotope effect seems to be primarily a second and third solvation shell effect. The ultimate experimental validation (or contradiction) of the predicted effect will allow us to better understand the accuracy of our microscopic simulation approach and to help lead the way to further refinements if necessary.

Acknowledgment. This research was supported by the Office of Naval Research. Computations were carried out at the Aeronautical Systems Center Major Shared Resource Center (ASC MSRC) at Wright-Patterson Air Force Base through a Department of Defense Grand Challenge Computing Grant and

at the National Center for Supercomputing Applications (NCSA) through NSF Metacenter Grant No. MCA94P017P. We also gratefully acknowledge the University Utah Center for High Performance Computing for a generous grant of Silicon Graphics Origin 2000 time.

References and Notes

(1) Straus, J. B.; Voth, G. A. *J. Phys. Chem.* **1993**, *97*, 7388.
(2) Straus, J. B.; Calhoun, A.; Voth, G. A. *J. Chem. Phys.* **1995**, *102*, 529.
(3) Calhoun, A.; Voth, G. A. *J. Phys. Chem.* **1996**, *100*, 10746.
(4) Calhoun, A.; Voth, G. A. *J. Electroanal. Chem.* **1998**, *253*, 450.
(5) Xia, X.; Berkowitz, M. L. *Chem. Phys. Lett.* **1994**, *227*, 561.
(6) Smith, B. B.; Halley, J. W. *J. Chem. Phys.* **1994**, *101*, 10915.
(7) Rose, D. A.; Benjamin, I. *Chem. Phys. Lett.* **1995**, *234*, 209.
(8) Schmickler, W. *J. Electroanal. Chem.* **1986**, *204*, 31.
(9) Schmickler, W. *Chem. Phys. Lett.* **1995**, *237*, 152.
(10) Koper, M. T. M.; Schmickler, W. *Chem. Phys.* **1996**, *211*, 123.
(11) Koper, M. T. M. *J. Phys. Chem. B* **1997**, *101*, 3168.
(12) Koper, M. T. M.; Mohr, J. H.; Schmickler, W. *Chem. Phys.* **1997**, *220*, 95.
(13) Curtiss, L. A.; Halley, J. W.; Hautman, J.; Hung, N. C.; Nagy, Z.; Rhee, Y. J.; Yonco, R. M. *J. Electrochem. Soc.* **1991**, *138*, 2032.
(14) Anderson, P. W. *Phys. Rev.* **1961**, *124*, 41.
(15) Newns, D. M. *Phys. Rev.* **1969**, *178*, 1123.
(16) Sebastian, K. L. *J. Chem. Phys.* **1989**, *90*, 5056.
(17) Ursenbach, C. P.; Voth, G. A. *J. Chem. Phys.* **1995**, *103*, 7569.
(18) Ursenbach, C. P.; Calhoun, A.; Voth, G. A. *J. Chem. Phys.* **1997**, *106*, 2811.
(19) Berne, B. J.; Thirumalai, D. *Annu. Rev. Phys. Chem.* **1986**, *37*, 401.
(20) Lobaugh, J.; Voth, G. A. *J. Chem. Phys.* **1997**, *106*, 2400.
(21) Wallqvist, A.; Berne, B. J. *Chem. Phys. Lett.* **1985**, *117*, 214.
(22) Kuharski, R. A.; Rossky, P. J. *J. Chem. Phys.* **1985**, *82*, 5164.
(23) DelBuono, G. S.; Rossky, P. J.; Schnitker, Y. *J. Chem. Phys.* **1991**, *95*, 3728.
(24) Billeter, S. R.; King, P. M.; van Gunsteren, W. F. *J. Chem. Phys.* **1994**, *100*, 6692.
(25) Gai, H.; Schenter, G. K.; Garrett, B. C. *J. Chem. Phys.* **1996**, *104*, 680.
(26) Gai, H.; Schenter, G. K.; Garrett, B. C. *Phys. Rev. B* **1996**, *54*, 14873.
(27) Berendsen, H. J.; Postma, J. P. M.; von Gunsteren, W. F.; Hermans, J. In *Intermolecular Forces*; Pullman, B., Ed.; Reidel: Dordrecht, 1981.
(28) Toukan, K.; Rahman, A. *Phys. Rev. B* **1985**, *31*, 2643.
(29) Raghavan, K.; Foster, K.; Motakabbir, K.; Berkowitz, M. *J. Chem. Phys.* **1991**, *94*, 2110.
(30) Spohr, E.; Heinzinger, K. *Ber. Bunsen-Ges. Phys. Chem.* **1988**, *92*, 1358.
(31) Spohr, E.; Heinzinger, K. *Chem. Phys. Lett.* **1986**, *123*, 218.
(32) Kuharski, R. A.; Bader, J. S.; Chandler, D.; Sprik, M.; Klein, M. L. *J. Chem. Phys.* **1988**, *89*, 3248.
(33) Bader, J. S.; Chandler, D. *Chem. Phys. Lett.* **1989**, *157*, 501.
(34) Bader, J. S.; Kuharski, R. A.; Chandler, D. *J. Chem. Phys.* **1990**, *93*, 230.
(35) Schmickler, W. *Interfacial Electrochemistry*; Oxford University Press: New York, 1996.
(36) Perram, J. W.; Ratner, M. A. *J. Chem. Phys.* **1996**, *104*, 5274.
(37) Tuckerman, M.; Berne, B. J.; Martyna, G. J. *J. Chem. Phys.* **1992**, *97*, 1990.
(38) Humphreys, D. D.; Friesner, R. A.; Berne, B. J. *J. Phys. Chem.* **1994**, *98*, 6885.
(39) Stuart, S. J.; Zhou, R.; Berne, B. J. *J. Chem. Phys.* **1996**, *105*, 1426.
(40) Nosé, S. *J. Chem. Phys.* **1984**, *81*, 511.
(41) Martyna, G. J.; Klein, M. L.; Tuckerman, M. *J. Chem. Phys.* **1992**, *97*, 2695.
(42) Chandler, D. *Introduction to Modern Statistical Mechanics*; Oxford University Press: New York, 1987.
(43) Kumar, S.; Douzida, D.; Swendsen, R. H.; Kollman, P. A.; Rosenberg, J. M. *J. Comput. Chem.* **1992**, *13*, 1011.
(44) Roux, B. *Comput. Phys. Commun.* **1995**, *91*, 275.
(45) Gregory, J. K. *Chem. Phys. Lett.* **1998**, *282*, 147.
(46) Cao, J.; Voth, G. A. *J. Chem. Phys.* **1994**, *100*, 5093.